Processing and characterization of effective copper molybdate hydrogen evolution catalyst

Majed Alshammari[1,*], Khulaif Alshammari[1], Sultan Alhassan[1], Alhulw H. Alshammari[1], Turki Alotaibi[1], Ahmed Iraqi[2], Taha Abdel Mohaymen Taha[1]

[1]Physics department, College of Science, Jouf University, P.O. Box:2014, Sakaka, Saudi Arabia
[2] Department of Chemistry, University of Sheffield, Sheffield, S3 7HF, United Kingdom

Email address; malshammary@ju.edu.sa

Abstract

The preparation and characterization of $Cu_{1.7}Mo_{0.3}O_4$ and $Cu_{1.4}Mo_{0.6}O_4$ nanostructures using the gelatin/sol-gel combustion method have been reported. The synthesized materials were investigated using X-ray diffraction (XRD), Fourier transform infrared spectroscopy (FTIR), scanning electron microscopy (SEM), surface area analysis, and optical measurements. UV-Vis absorption spectra of the nanocomposites were analysed to investigate the absorption and bandgap energy of the optical band gap. The $Cu_{1.7}Mo_{0.3}O_4$ nanomaterial show cased a triclinic crystal structure system, while the $Cu_{1.4}Mo_{0.6}O_4$ exhibited an orthorhombic system. The BET surface area analysis of the catalysts has values of 53 and 502 m^2/g. The $Cu_{1.7}Mo_{0.3}O_4$ sample proved to be the most active in generating hydrogen through $NaBH_4$ methanolysis, displaying an impressive production rate of 23063 mL/g.min. The findings indicate that the addition of $Cu_{1.7}Mo_{0.3}O_4$ improves the catalytic activity of the methanolysis reaction involving sodium borohydride.

Keywords: Hydrogen energy; copper molybdate; Catalyst; $NaBH_4$; Optical band gap

1. Introduction

Prior to the industrial revolution of the 18th century, energy was mostly derived from human muscles, wind (e.g., windmills), animals (e.g., horses), and water (e.g., watermills). With the invention of the engine, humanity seek alternate energy resources like coal, fossil fuels, and natural gas to power their revolution. Unfortunately, these sources are ultimately unsustainable since their extraction and consumption rates vastly outpace their fossil-fuel generation rates. Indeed, as an advanced energy source, hydrogen exhibit the potentiality to be a viable substitute for fossil fuels [1,2]. Hydrogen gas can be stored in two forms; molecular hydrogen (used in pressurised vessels and liquid hydrogen tanks) and by atomic hydrogen (which includes metal hydrides) [3].

The present energy infrastructure, which is mainly based on fossil fuels, has been recognized as a significant contributor in the onset of global climate change and the emergence of local air contamination [4]. Fuel cells that run on hydrogen (H_2) have substantial environmental benefits [5]. However, implementing a hydrogen-based economy on a national or global scale presents significant scientific and technological obstacles [6]. Several technologies have been developed to address the storage and delivery of pure H_2 including compressed gas [7], cryogenic liquid [8], adsorption on carbon materials [9], metal hydrides [10], and chemical hydrides [11]. These storage systems were examined, with a focus on their potential for enhancement as well as their physical limitations [12]. Sodium borohydride (NaBH4), among other chemical hydrides, stands out as a promising storage material for delivering H_2 gas to fuel cells due to its enormous hydrogen storage capacity (10.8 wt%) and potentially safe operation [13]. The mechanisms for evolving stored H_2 from NaBH4 comprise methanolysis and hydrolysis [3], or by a combination of the two mechanisms [14].

In recent times, researchers have focused on the generation of hydrogen utilising metal hydrides such as ($NaBH_4$) [15], lithium hydride (LiH) [16], and lithium borohydride ($LiBH_4$) [17]. However, due to its ability to reuse byproducts, high hydrogen density, and purity of the developed hydrogen, $NaBH_4$ has emerged as the most efficient metal hydride for hydrogen generation [18]. Additionally, $NaBH_4$ cannot be employed directly, a new catalyst must be used to speed hydrogen production, enhance reaction rate, as well as decrease activation energy [19]. Hence, metal oxides exhibit exceptional catalytic properties for NaBH4 hydrolysis, making them highly efficient catalysts. Numerous metal oxides, such as Ni, Zn, Co, Cu, Pt, Ti, Al, among others, have been extensively investigated and analyzed for their exceptional physical and chemical characteristics [20-22]. Numerous studies have explored the performance of metal catalysts for hydrogen production, yielding variable results. For instance, in a study by Amutha et al. [23], it was demonstrated that ionic liquid-functionalized graphene oxide, loaded with CuO nanostructures, exhibited exceptional catalytic activity for H2 generation from NaBH4. Furthermore, Saka et al. [24] reported the use of NaBH4 and metal catalysts, such as CuB, for hydrogen production, which showed improved performance of the metal catalysts during NaBH4 methanolysis. In addition, various catalysts have been examined for their hydrogen production capabilities. For example, a Ni/TiO_2 catalyst material, fabricated via the sol-gel approach, attained a hydrogen production rate of 110.87 mL/g·min [25]. Other catalysts, including Co_3O_4 microcubes (1497 mL/g·min) [26], Co_3O_4 nanorods (1776 mL/g·min) [27], Co_3O_4 nanofoams (1930 mL/g·min) [28], and FeCuCo materials (1380 mL/g·min) [29], also exhibited varying production rates. However, there are still some research gaps in this area. One research gap is the need for catalysts that are both efficient and cost-effective. While some catalysts have shown high catalytic activity, they may also be expensive or require toxic materials. Another research gap is the need for catalysts that can maintain their catalytic activity over multiple cycles. Some catalysts have shown good initial activity, but

their performance decreases significantly after a few cycles. Additionally, the mechanisms of the catalytic reactions involved in sodium borohydride methanolysis are not fully understood, and further research is needed to elucidate these mechanisms. Overall, future research should focus on developing catalysts that are both efficient and cost-effective, have good durability, and have a clear understanding of the catalytic mechanisms involved.

In this work, we investigate the fabrication and characterization of $Cu_{1.7}Mo_{0.3}O_4$ and $Cu_{1.4}Mo_{0.6}O_4$ nanostructures using the gelatin/sol-gel combustion method. Two different concentrations, 0.3 and 0.6, were utilized to investigate their effect on the structural, morphological, and optical characteristics of the nanocomposites. The synthesized materials were investigated using X-ray diffraction (XRD), Fourier transform infrared spectroscopy (FTIR), scanning electron microscopy (SEM), surface area analysis, and optical measurements. The measurements included UV-Vis spectroscopy, which provides information about the absorption and bandgap energy of the nanocomposites. In conclusion, the catalytic performance of these nanocomposites was fully assessed for the hydrogen evolution process during the methanolysis of sodium borohydride

2. Experimental

2.1 Materials

For the synthesis of $Cu_{1.7}Mo_{0.3}O_4$ and $Cu_{1.4}Mo_{0.6}O_4$ nanostructures we have used copper(II) chloride ($CuCl_2.2H_2O$, $\geq$ 99.0%, Sigma-Aldrich), ammonium heptamolybdate tetrahydrate ((NH_4)$_6Mo_7O_{24}.4H_2O$, $\geq$ 99.3%, Loba Chemie, India) and gelatin (technical grade, Loba Chemie, India). All materials were used without requiring additional treatment.

2.2 Materials fabrication

The sol-gel approach is a versatile and scalable method for the synthesis of nanomaterials. The nanoparticles produced by this method are typically uniform in size and have a high surface area. Different nanoparticles fabricated by the sol-gel approach have been shown to have good

catalytic activity for a variety of reactions, comprising the oxygen evolution reaction (OER) and the hydrogen evolution reaction (HER). Accordingly, we have used the gelatin/sol-gel combustion method for the preparation of $Cu_{1.7}Mo_{0.3}O_4$ and $Cu_{1.4}Mo_{0.6}O_4$ nanostructures. The precursor solution is typically prepared by dissolving stoichiometric amounts of $CuCl_2.2H_2O$ and $(NH_4)_6Mo_7O_{24}.4H_2O$ in deionized water. A gelatin solution was introduced to the metal solution. The ratio of metals to gelatin in the solution was 1:2. The blend was stirred for 2 h at 80 °C. The metal ions will then react with each other and with the solvent to form a gel. After the gel has formed, it is dried in an oven at a temperature of 260 °C. The drying process removes the solvent and other volatile components from the gel, leaving behind a solid xerogel. The xerogel is then calcined at a temperature of 500 °C to form the $Cu_{1.7}Mo_{0.3}O_4$ and $Cu_{1.4}Mo_{0.6}O_4$ nanostructures. The calcination process removes any remaining organic matter from the xerogel and converts the metal precursors to their oxides.

2.3 Materials Characterization

The XRD was analysed using a Shimadzu 7000 XRD to identify the phases present in the sample and to determine their crystal structure. The Shimadzu 100-FTIR tracer was used to analyse the ATR spectra of $Cu_{1.7}Mo_{0.3}O_4$ and $Cu_{1.4}Mo_{0.6}O_4$ nanostructures. The morphological characteristics of the nanostructures are then investigated using Quattro S scanning electron microscopy (SEM) technique. The BET surface area is an important parameter for nanostructures because it affects their catalytic activity and other properties. The Novae401 surface area analyzer is a rapid and accurate method for measuring the BET surface area of $Cu_{1.7}Mo_{0.3}O_4$ and $Cu_{1.4}Mo_{0.6}O_4$ nanostructures. The UV-Vis optical absorption spectra of the nanostructures were analyzed by Evo201 UV-Vis spectrometer to determine their optical properties.

2.4 Hydrogen evolution activity

NaBH$_4$ hydrolysis carried out at 30 °C in methanol. Hydrolysis was assisted by adding a catalyst into the NaBH$_4$ solution. Catalysts are substances decreasing activation energies of reactions making reactions fast. The quantity of catalyst utilized (0.02 grams) together with 0.25 grams of NaBH$_4$. This blend was then moved to a glass reactor. Thereafter, methanol 10 ml was added quickly. Using water displacement is a quick and accurate way for volumetric measurement of hydrogen gas. The collecting of gases within a container submerged in water is what makes water displacement possible. Therefore, this amount of water can be taken to have replaced any volume of the gas hence its value must remain equivalent to the H$_2$ gas volume. The experimental data of hydrogen production for Cu$_{1.7}$Mo$_{0.3}$O$_4$ and Cu$_{1.4}$Mo$_{0.6}$O$_4$ at different mass of catalyst, mass of NaBH$_4$ and temperature was completed. Finally, the reusability test data for the Cu$_{1.7}$Mo$_{0.3}$O$_4$ catalyst was performed after undergoing 5 reusability cycles.

3. Results and discussion

The X-ray diffraction (XRD) technique has been widely utilized as an essential method for identifying the crystal structure of compounds. Accordingly, XRD was used where its pattern for the Cu$_{1.7}$Mo$_{0.3}$O$_4$, and Cu$_{1.4}$Mo$_{0.6}$O$_4$ samples is shown in the Fig. 1. The CuMoO$_4$ related main peaks are clearly indexed at 2θ= 13.04º, 15.98º, 23.9º, 26.5º, and 32.98º, these peaks are due to the existing planes of (-101), (101), (201), (-202), and (-302) respectively [30,31]. The main peaks and the rest of the peaks matched those in the JCPDS card number 73-0488 which indicates the triclinic crystal structure system of Cu$_{1.7}$Mo$_{0.3}$O$_4$.
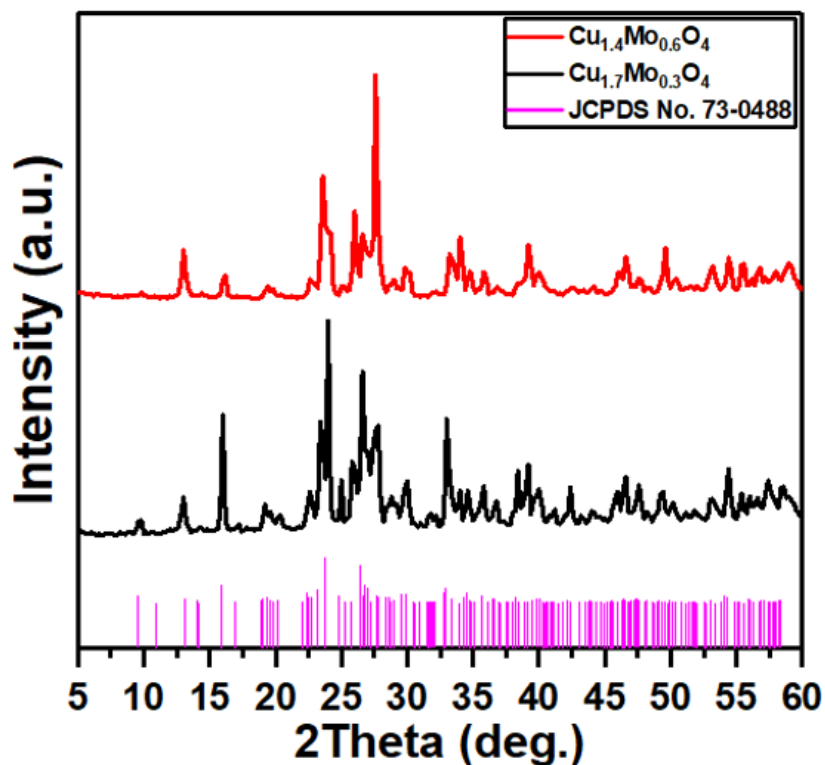
Fig. 1 The XRD diffraction patterns of $Cu_{1.7}Mo_{0.3}O_4$, and $Cu_{1.4}Mo_{0.6}O_4$ nanostructures.

The XRD peaks for $Cu_{1.4}Mo_{0.6}O_4$ sample are shown in Fig. 1 as well. The main peak was shifted to higher $2\theta = 27.2°$ which is corresponding to (140) plane. All the appeared peaks in the $Cu_{1.4}Mo_{0.6}O_4$ sample have full agreements with those related to orthorhombic system in the card number 00-022-0609. It is clear, the crystal structure was transformed to orthorhombic system when the content of Cu decreased from 1.7 to 1.4 and Mo increased from 0.3 to 0.6. The successful preparation of $Cu_{1.7}Mo_{0.3}O_4$, and $Cu_{1.4}Mo_{0.6}O_4$ is confirmed since the crystal structure has changed upon increasing the content of Cu and decreasing Mo.

The Debye-Scherrer (equation (1)) was utilized to calculate the mean crystal size of the $Cu_{1.7}Mo_{0.3}O_4$, and $Cu_{1.4}Mo_{0.6}O_4$ nanostructures [32,33];

$$D = \frac{0.9\lambda}{\beta \cos\theta} \qquad (1)$$

The D indicates the crystalline size, λ and β refers to the Xray wavelength of 0.154056 nm and Full width at half maximum of the XRD diffraction peaks respectively. The mean

7

crystalline size was obtained from the broadest three peaks in the $Cu_{1.7}Mo_{0.3}O_4$ sample and found to be 32.7 nm while 60.5 nm for $Cu_{1.4}Mo_{0.6}O_4$. The increase in the crystal size is expected since we increase the molybdenum over copper that has relatively lower atomic radius.

Figure 2 displays the FTIR spectra ranging from 400 to 1500 cm^{-1} for both $Cu_{1.7}Mo_{0.3}O_4$ and $Cu_{1.4}Mo_{0.6}O_4$. The absorption bands that are related to $CuMoO_4$ are below 1000 cm^{-1}. In the $Cu_{1.7}Mo_{0.3}O_4$, various absorption bands were appeared as following. The Mo-O-Mo vibration mode is presented at the absorption band of 819 cm^{-1} [34]. The absorption peaks located at 795 cm^{-1}, 900 cm^{-1}, and 938 cm^{-1} are related to stretching mode of asymmetric Mo–O [35]. In comparison between $Cu_{1.7}Mo_{0.3}O_4$, and $Cu_{1.4}Mo_{0.6}O_4$ samples, one additional absorption band at 484 cm^{-1} was appeared in $Cu_{1.4}Mo_{0.6}O_4$ due to MoO_3 bending mode as well as stretching vibration of square planar CuO_4 [35]. The Cu–O–Mo stretching mode caused the band at 700 cm^{-1} [36] which evidence the formation of copper molybdenum oxide.
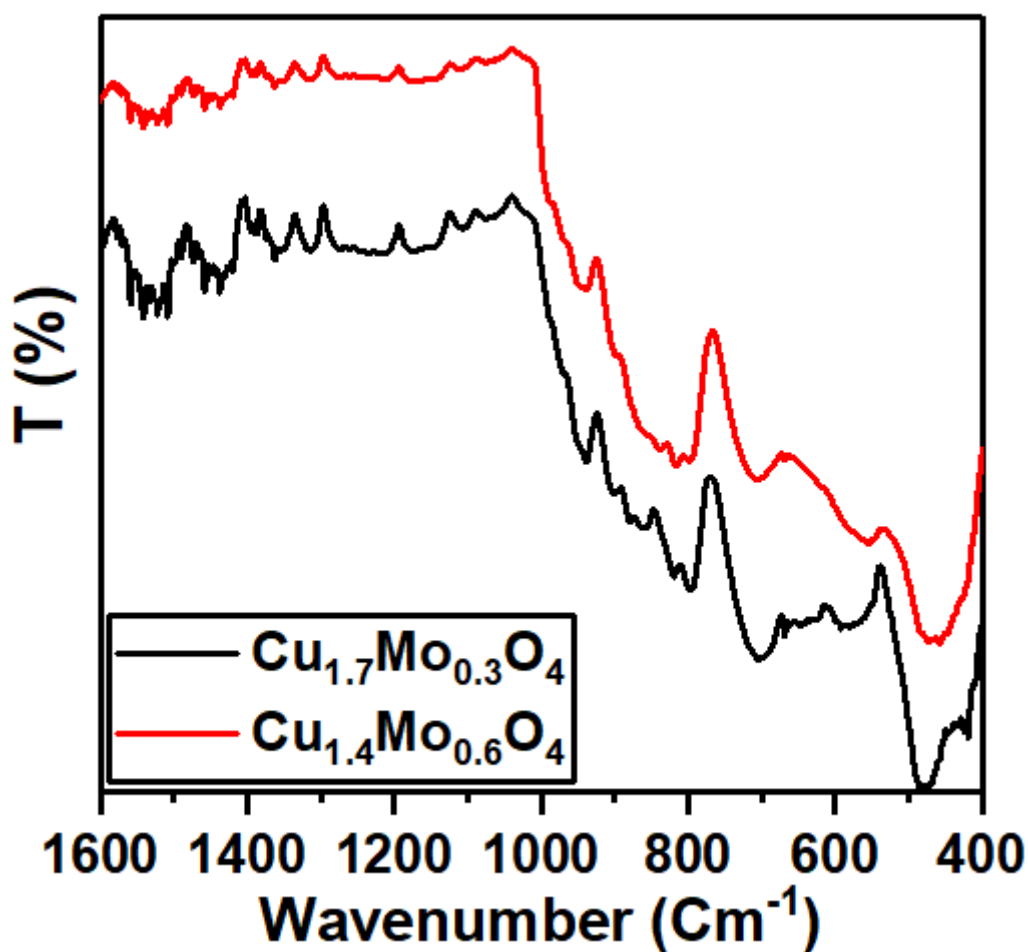
Fig. 2 The FTIR spectra for the $Cu_{1.7}Mo_{0.3}O_4$, and $Cu_{1.4}Mo_{0.6}O_4$ nanostructures.

The SEM morphology of $CuMoO_4$ orthorhombic crystals can exhibit variations depending on the specific synthesis approach and conditions employed during the process. The SEM images of $Cu_{1.7}Mo_{0.3}O_4$, and $Cu_{1.4}Mo_{0.6}O_4$ nanostructures shown in Fig. 3a,b have a plate-like morphology with a smooth surface.
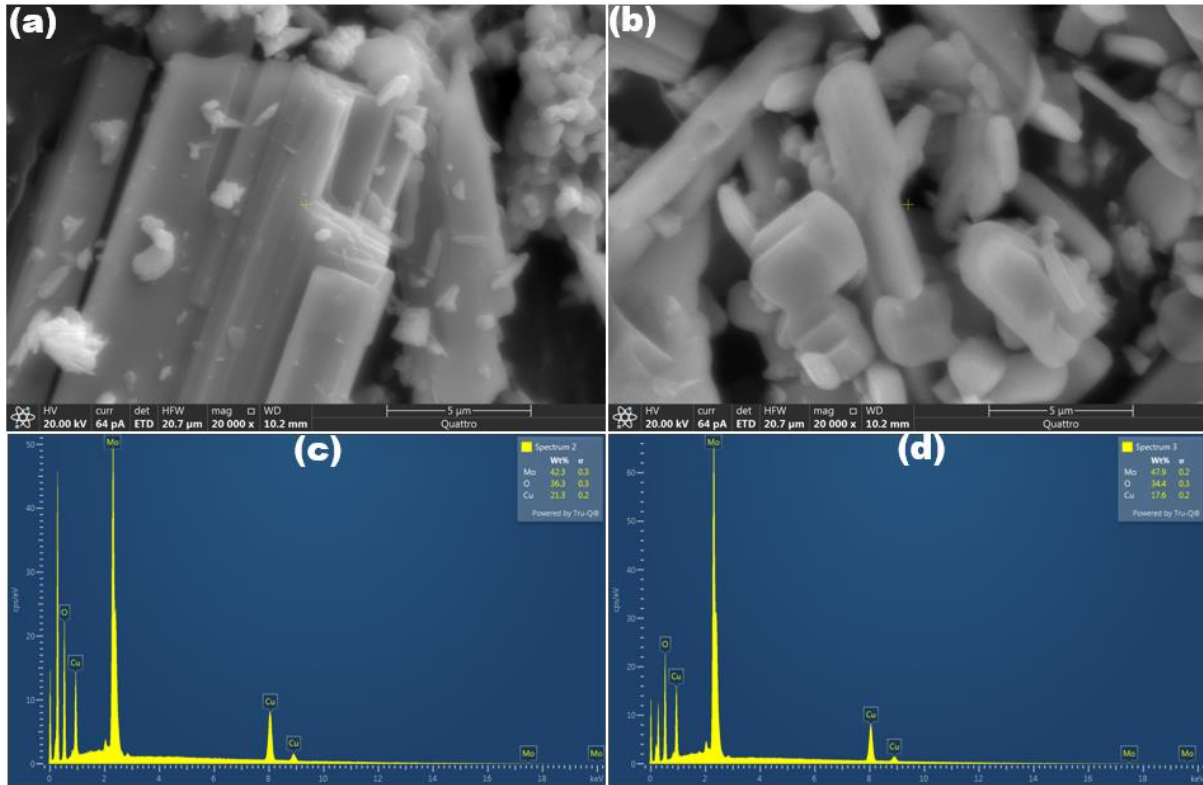
Fig. 3 The SEM micrographs of (a) $Cu_{1.7}Mo_{0.3}O_4$, (b) $Cu_{1.4}Mo_{0.6}O_4$, EDS of (c) $Cu_{1.7}Mo_{0.3}O_4$ and (d) $Cu_{1.4}Mo_{0.6}O_4$ nanostructures.

Confirmation of copper (Cu), molybdenum (Mo), and oxygen (O) in the crystal structure of $Cu_{1.7}Mo_{0.3}O_4$ and $Cu_{1.4}Mo_{0.6}O_4$ was achieved through EDS analysis. The relative abundance of these elements is quantified in Fig. 3(c, d), and the corresponding weight percentages are provided in Table 1. These results affirm the successful preparation of $Cu_{1.7}Mo_{0.3}O_4$ and $Cu_{1.4}Mo_{0.6}O_4$ samples

Table 1 EDS analysis results of $Cu_{1.7}Mo_{0.3}O_4$, and $Cu_{1.4}Mo_{0.6}O_4$ crystals

Sample	Element	Wt%
$Cu_{1.7}Mo_{0.3}O_4$	O	36.34
	Cu	21.33
	Mo	42.33
$Cu_{1.4}Mo_{0.6}O_4$	O	34.43
	Cu	17.62
	Mo	47.94

Fig.4a illustrates the nitrogen isotherms at 77K. It is noteworthy that all the samples prepared demonstrate type IV isotherms featuring an H4 hysteresis loop, aligning with the IUPAC classification. This observation indicates the mesoporous texture of the prepared samples. The surface area of $Cu_{1.7}Mo_{0.3}O_4$ is estimated to be 56.96 m²/g, while that of $Cu_{1.4}Mo_{0.6}O_4$ is measured at 81.26 m²/g. Additionally, the pore volume exhibited an upward trend in correspondence with the surface area behavior. Specifically, the pore volume for $Cu_{1.7}Mo_{0.3}O_4$ is recorded as 0.07315 cm³/g, while for $Cu_{1.4}Mo_{0.6}O_4$, it is measured at 0.1135 cm³/g. The BJH average pore diameters of the samples ranged from 2.5 to 15 nm, as depicted in Fig.4b. This range further emphasizes the existence of mesoporous structures. Notably, the distribution curve for the $Cu_{1.4}Mo_{0.6}O_4$ sample shifted towards the most abundant mesoporous structure, contributing to its higher surface area. The boost in surface area could be due to the mesoporous structures, which are characterized by pores with diameters typically ranging from 2 to 50 nm. These structures contribute significantly to the overall surface area as they provide a larger surface for interactions with other substances.
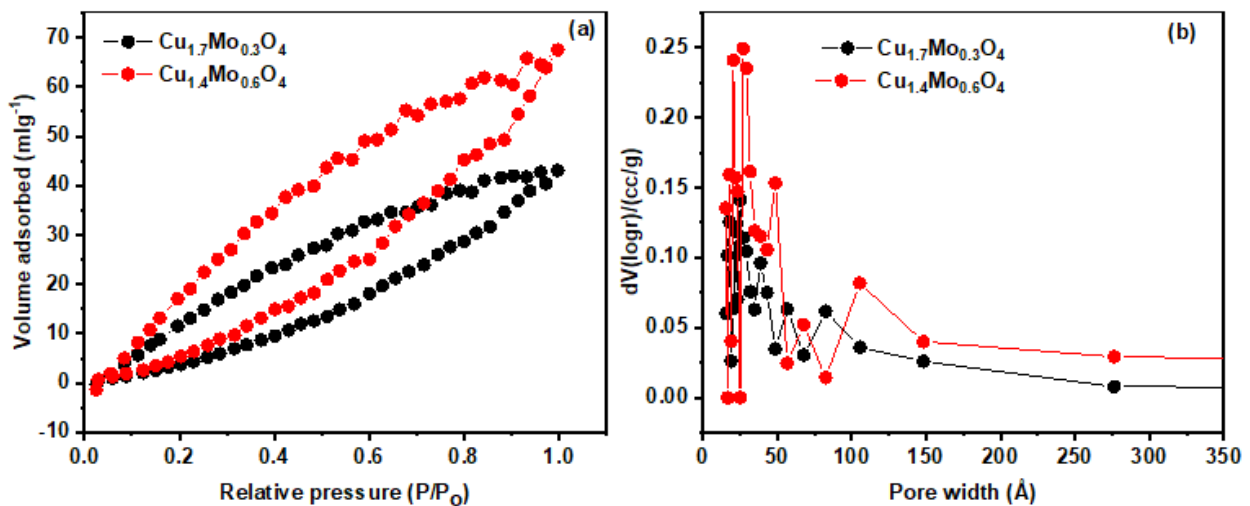

Fig. 4 (a) The nitrogen isotherm, and (b) pore size distribution of the $Cu_{1.7}Mo_{0.3}O_4$, and $Cu_{1.4}Mo_{0.6}O_4$ nanostructures.

The big surface area of $Cu_{1.4}Mo_{0.6}O_4$ provides a large number of active sites for catalytic reactions. The surface area and pore size of catalyst supports have a significant impact on hydrogen catalytic performance. The surface area of the support material is closely related to the rate-limiting mechanisms and restriction degrees of the reaction [37]. For example, in CO_2 hydrogenation reactions, catalysts with pore sizes of 7-10 nm and corresponding Fe_2O_3 particle sizes of 5-8 nm showed the highest activity [38]. Additionally, the size of Rh particles in silica supports influenced the catalytic activity, with smaller Rh particles maintained inside supports with larger pore sizes [39]. The surface area of the catalyst also plays a crucial role, as higher surface areas lead to higher catalytic activity. Therefore, the combination of larger pore sizes, smaller particle sizes, and higher surface areas in catalyst supports can enhance hydrogen catalytic performance.

Optical absorption has been found to have an effect on hydrogen catalytic performance. The presence of subsurface hydrogen (H_2) can significantly increase or decrease the bond energy and reactivity of adsorbed hydrogen depending on the metal [40]. Additionally, the catalytic activity of noble metals such as Pd, Ni, Cu, and Ag for hydrogen sorption has been studied using an optical technique [41,42]. The uptake rate of hydrogen is limited by chemisorption, as deduced by kinetic modeling [43]. The calculated activation energy for catalytic activity is dependent on the oxygen concentration, exhibiting a minimum value at the highest oxygen content. [44]. These findings suggest that optical absorption can influence the catalytic activity and kinetics of hydrogen sorption processes.

The optical properties of $Cu_{1.7}Mo_{0.3}O_4$ and $Cu_{1.4}Mo_{0.6}O_4$ nanostructures has been investigated at different wavelengths from 190 to 800 nm. Fig. 5a show the normalized absorbance versus the wavelength for these nanostructures. The absorption spectra of the two samples bands showed bands at 450 and 500 nm that results from extrinsic transitions caused by defects in structure [45].

The optical band gap is defined as the energy difference between valence (VB) and conduction band (CB). This energy, minimum amount, is required to transfer the electron from VB to CB. The optical band gap is determined to investigate the electronic structure of $Cu_{1.7}Mo_{0.3}O4$ and $Cu_{1.4}Mo_{0.6}O4$. To calculate the band gap, the Taus formula was used as follows [46,47];

$$\alpha h\upsilon = A(h\upsilon - E_{opt})^{0.5} \qquad\qquad (2)$$

Here, α represents the absorption coefficient, h is Planck's constant, v denotes the frequency of the light, A is a constant, and E_{opt} signifies the band gap
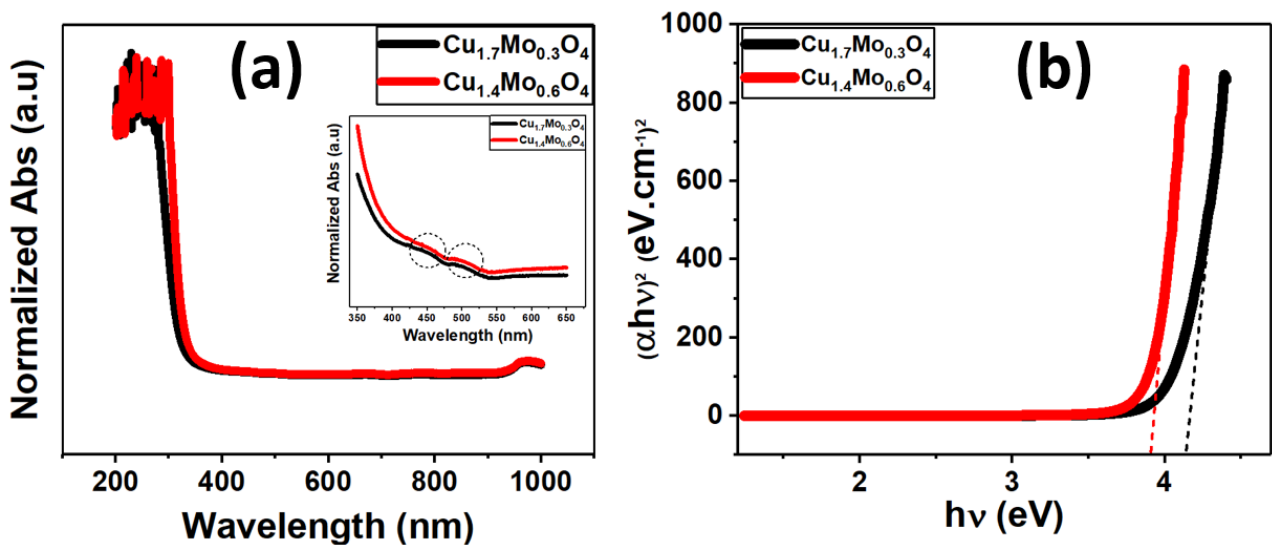

Fig. 5 Plots of (a) normalized absorbance against wavelength; the inset showed the absorption bands at 450 and 500 nm and (b) $(\alpha h\upsilon)^2$ against (hv) for $Cu_{1.7}Mo_{0.3}O_4$ and $Cu_{1.4}Mo_{0.6}O_4$.

A linear in region is represented in Fig. 5b for $Cu_{1.7}Mo_{0.3}O_4$ and $Cu_{1.4}Mo_{0.6}O_4$. This Figure shows $(\alpha h\upsilon)^2$ on y-axis versus $(h\upsilon)$ on x-axis. In order to obtain the optical band gap E_{opt}, we extrapolate the linear part of the plot on x-axis $(h\upsilon)$ in eV unit. The E_{opt} is approximately 4.14 eV for $Cu_{1.7}Mo_{0.3}O_4$, while 3.91 eV for $Cu_{1.4}Mo_{0.6}O_4$. The redaction of band gap could be from the change in morphological, surface structure and the particle size [48]. The band gap determines the energy required to create these pairs. If the band gap is too small, the electron-hole pairs may recombine before they can participate in the hydrogen production reaction.

Therefore, a larger band gap is generally preferred to promote charge separation and prevent recombination [49,50].

The self-decomposition process of sodium borohydride in a solution containing methanol has garnered significant attention due to its notable stability and ability to operate at low temperatures. Furthermore, this process exhibits a quick and substantial production of hydrogen gas, as shown by previous research [51]. Consequently, the reaction mentioned above was used to evaluate the efficacy of $Cu_{2-x}Mo_xO_4$ nanocomposites as a catalyst for the release of hydrogen from sodium borohydride ($NaBH_4$). In the beginning, the measurement of the hydrogen gas volume was conducted at different time intervals at a temperature of 303 K. The figure 6 shows the hydrogen volume curves at various time intervals for the $Cu_{1.7}Mo_{0.3}O_4$ and $Cu_{1.4}Mo_{0.6}O_4$ samples.
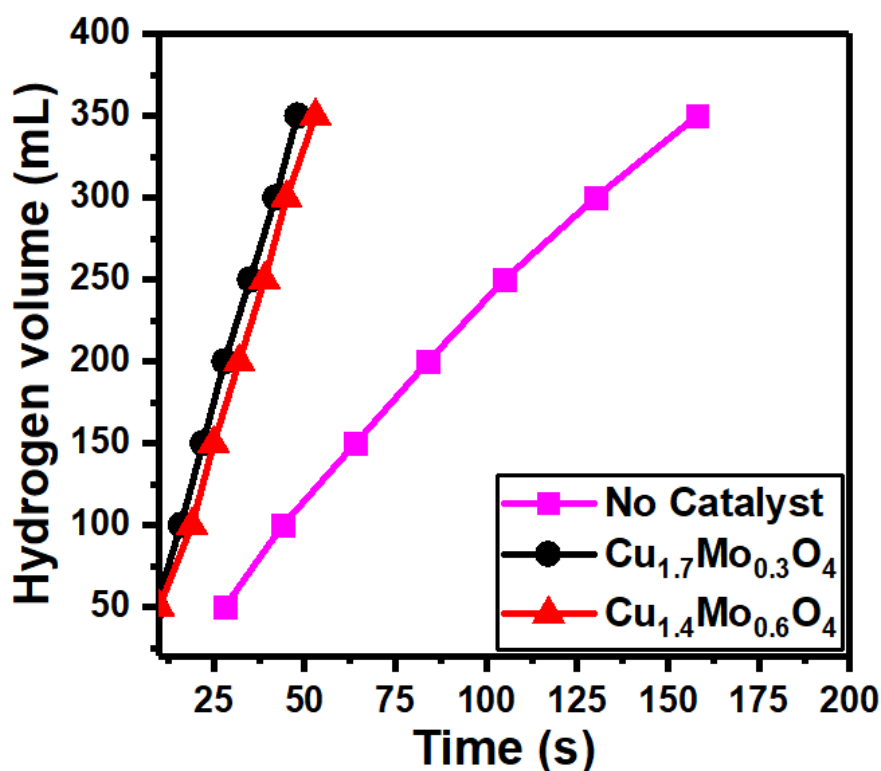
Fig. 7 The change in volume of hydrogen over time for $Cu_{1.7}Mo_{0.3}O_4$ and $Cu_{1.4}Mo_{0.6}O_4$ catalysts.

According to Figure 6, the rate of producing hydrogen exhibits enhancement with a decrease in the proportion of molybdenum. This effect arises because of a drop in the number of active

14

sites after the increase of molybdenum concentration [52]. The active sites are significant in determining the performance of a catalysts. Also, in Figure 7, it can be shown that time needed to produce hydrogen via the process of $NaBH_4$ methanolysis significantly decreases after the occurrence of the catalytic reaction. The $Cu_{1.7}Mo_{0.3}O_4$ sample demonstrated the highest level of activity in terms of hydrogen production.

The hydrolysis of $NaBH_4$, leading to the production of H_2, is postulated to occur via a sequence of two kinetic stages in the presence of metal catalysts. In the first phase, the $Cu_{1.7}Mo_{0.3}O_4$ and $Cu_{1.4}Mo_{0.6}O_4$ catalysts undergo chemisorption with BH_4 ions. During the second stage, the release of hydrogen gas occurs at the catalyst's surface [53]. Hence, as the surface of the catalyst adsorbs a greater number of BH_4 ions, there will be an increase in its catalytic activity. The findings of this study indicate that the addition of $Cu_{1.7}Mo_{0.3}O_4$ enhances the catalytic efficiency of the methanolysis reaction involving $NaBH_4$. The bimolecular Langmuir-Hinshelwood model is frequently employed to elucidate the reaction mechanisms underlying the hydrolysis of NaBH4. This model encompasses two crucial steps: the adsorption of reactants onto the catalyst surface and the subsequent reaction of the adsorbed species [54]. To gain a deeper understanding of the catalytic behaviour involved in hydrogen synthesis, this study primarily investigates the examination of the generation rate (k). The provided equation indicates that the production rate is influenced by factors such as hydrogen volume (V), catalyst mass (mcat), and reaction time (t) [55,56];

$$k = \frac{V}{t.m_{cat}} \tag{3}$$

A comparison of the rate of hydrogen evolution from $NaBH_4$ hydrolysis using $Cu_{1.7}Mo_{0.3}O_4$ and $Cu_{1.4}Mo_{0.6}O_4$ is shown in Fig. 8. The slopes of the straight lines, as depicted in Fig. 7, were calculated to get the values for hydrogen production (*k*). The results showed that these values were 23063 and 21494 mL/g.min. The $Cu_{1.7}Mo_{0.3}O_4$ sample demonstrated the highest rate of

production, suggesting a boost in the number of active centers on the sample surface. A significant amount of hydrogen gas is promptly released from the catalyst $Cu_{1.7}Mo_{0.3}O_4$, which has an increased attraction to BH_4 ions at its surface sites.
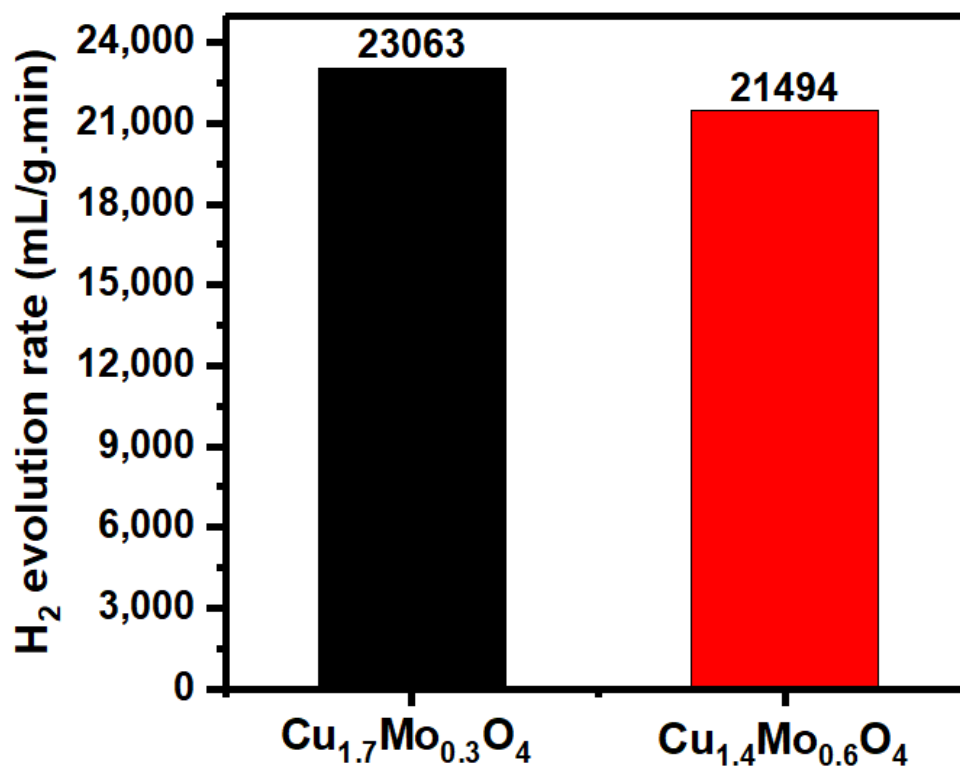
Fig. 8: The rate hydrogen production for $Cu_{1.7}Mo_{0.3}O_4$ and $Cu_{1.4}Mo_{0.6}O_4$ samples.

The hydrogen production rate exhibits variation among various catalysts, as shown by the given results. The following table 1 presents a comparison of the different results with this finding:

Table 1: A comparison of the hydrogen production rates using different catalysts in this study.

Catalyst	Type	r (mL/g.min)	Ref.
$CoB/Ag–TiO_2$	Powder	393	[57]
Co–Mo–B/C	Powder	1280	[58]
$CuCo_2O$	Powder	1370	[59]
Co-Cu-Fe	Foam	1380	[29]
$CuFe_2O_4$	Powder	1810	[46]
Co-Cu-Ni	Powder	5100	[60]
$Fe_3O_4/FeS_2/g-C_3N_4$	Powder	8480	[47]
$Cu_{1.7}Mo_{0.3}O_4$	Powder	23063	This study

The hydrogen production rate presented in Table 1 reveal that the sample $Cu_{1.7}Mo_{0.3}O_4$ exhibits superior performance compared to different other catalysts. The findings of the study demonstrated that the introduction of only a small amount of sodium significantly enhanced the catalytic performance.

The data presented in Fig. 9 illustrates the hydrogen production for $Cu_{1.7}Mo_{0.3}O_4$ and $Cu_{1.4}Mo_{0.6}O_4$ at various masses of both catalyst and $NaBH_4$. Hydrogen production exhibits variations dependent on the catalyst, mass of the catalyst, and mass of $NaBH_4$. Generally, increased masses of both catalyst and $NaBH_4$ result in higher hydrogen production. This observed behaviour aligns with findings reported in the literature [61-63].
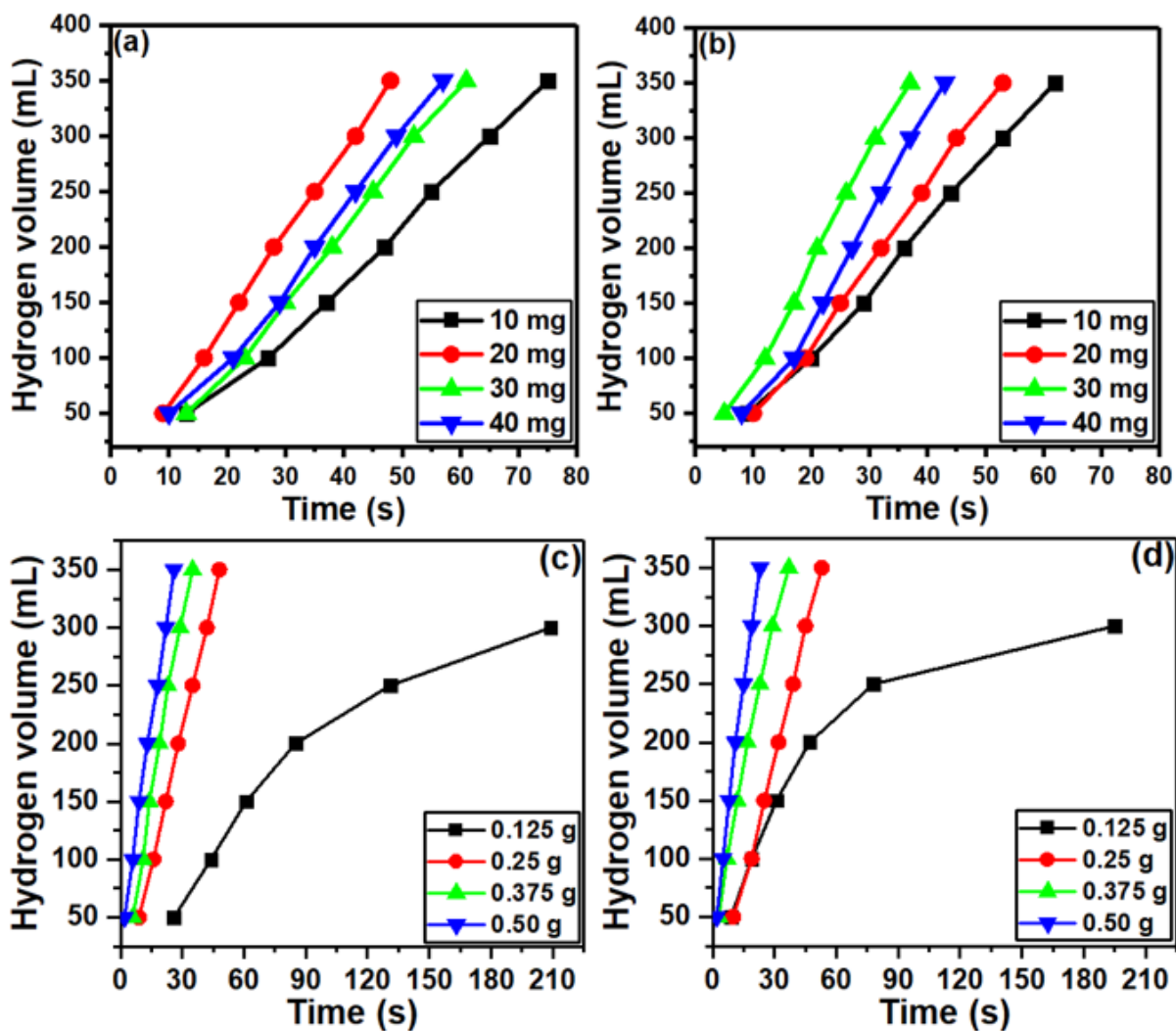
Fig. 9: The experiment data of hydrogen production for $Cu_{1.7}Mo_{0.3}O_4$ and $Cu_{1.4}Mo_{0.6}O_4$ at different (a), (b) mass of catalyst, (c) and (d) mass of $NaBH_4$.

The effect of temperature on hydrogen production for $Cu_{1.7}Mo_{0.3}O_4$ and $Cu_{1.4}Mo_{0.6}O_4$ is given in Fig. 10. For both catalysts, higher temperatures generally lead to higher hydrogen production. Higher temperatures can enhance the mixing of reactants and improve the diffusion of $NaBH_4$ species towards the active centers on the catalyst, facilitating faster reaction rates.
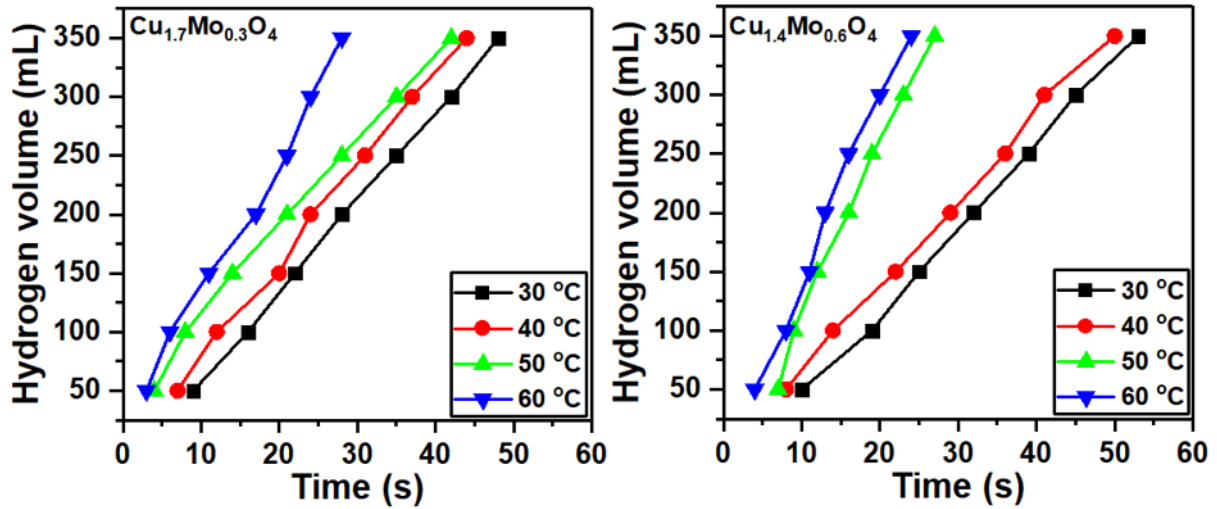
Fig. 10: The experiment data of hydrogen production for $Cu_{1.7}Mo_{0.3}O_4$ and $Cu_{1.4}Mo_{0.6}O_4$ at different temperatures.

According to the Arrhenius equation [64], the reaction rate increases exponentially with temperature due to an increase in the average kinetic energy of the reactants. This allows them to overcome the activation energy barrier more easily and collide more frequently, leading to more frequent reactions.

$$k = A\, exp(-E_a/(RT)) \qquad (4)$$

where A is the pre-exponential factor, E_a represents the activation energy, and the ideal gas constant R has the value of 8.314 J/mol.K. The Arrhenius equation can be rearranged to plot the natural logarithm of the rate constant (ln(k)) against the reciprocal of temperature (1000/T), as shown in Fig 11. This leads to a linear relationship with a slope of (-Ea /R), enabling the determination of the activation energy.

Fig. 11: Plots of (ln(k)) against the reciprocal of temperature (1000/T) for $Cu_{1.7}Mo_{0.3}O_4$ and $Cu_{1.4}Mo_{0.6}O_4$ catalysts.
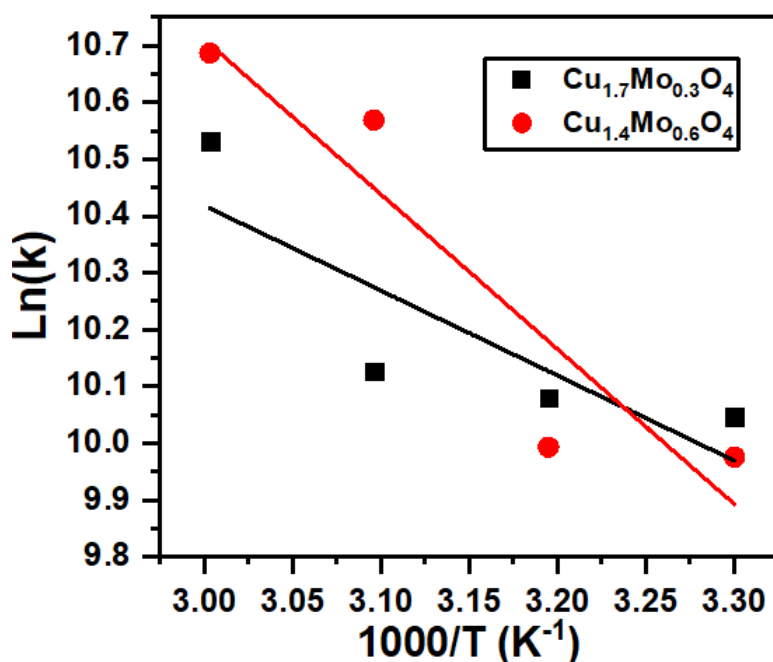
The activation energies of $Cu_{1.7}Mo_{0.3}O_4$ and $Cu_{1.4}Mo_{0.6}O_4$ catalysts were calculated to be 12.42 and 22.64 kJ/mol. Obviously, $Cu_{1.7}Mo_{0.3}O_4$ has a significantly lower activation energy compared to $Cu_{1.4}Mo_{0.6}O_4$. This means that $Cu_{1.7}Mo_{0.3}O_4$ requires less energy for $NaBH_4$ molecules to overcome the activation barrier and participate in the reaction. The deviation from the Arrhenius equation as depicted in Fig. 11, could be attributed to the catalytic reactions often involve intricate multi-step processes with varying activation energies, leading to deviations from the expected temperature dependence. Additionally, surface phenomena play a significant role in catalytic reactions, influencing reaction rates through factors such as active site availability and adsorption/desorption processes. Changes in surface properties or restructuring can lead to deviations from Arrhenius behavior. Furthermore, catalyst deactivation, whether through poisoning, sintering, or fouling, can also disrupt the expected temperature dependence by altering the catalyst's activity over time. Finally, non-ideal conditions such as non-uniform temperature distributions or variations in reactant concentrations can contribute to deviations from idealized behavior [65, 66].

The reusability test data for the $Cu_{1.7}Mo_{0.3}O_4$ catalyst is plotted in Fig. 12. The $Cu_{1.7}Mo_{0.3}O_4$ catalyst experiences a decrease in efficiency from 100% to 82% after undergoing 5 reusability cycles at 30°C. Over repeated reaction cycles, the high temperatures involved in $NaBH_4$ methanolysis could cause the catalyst nanoparticles to coalesce and grow larger, reducing their surface area and active sites. This can lead to a decrease in efficiency.
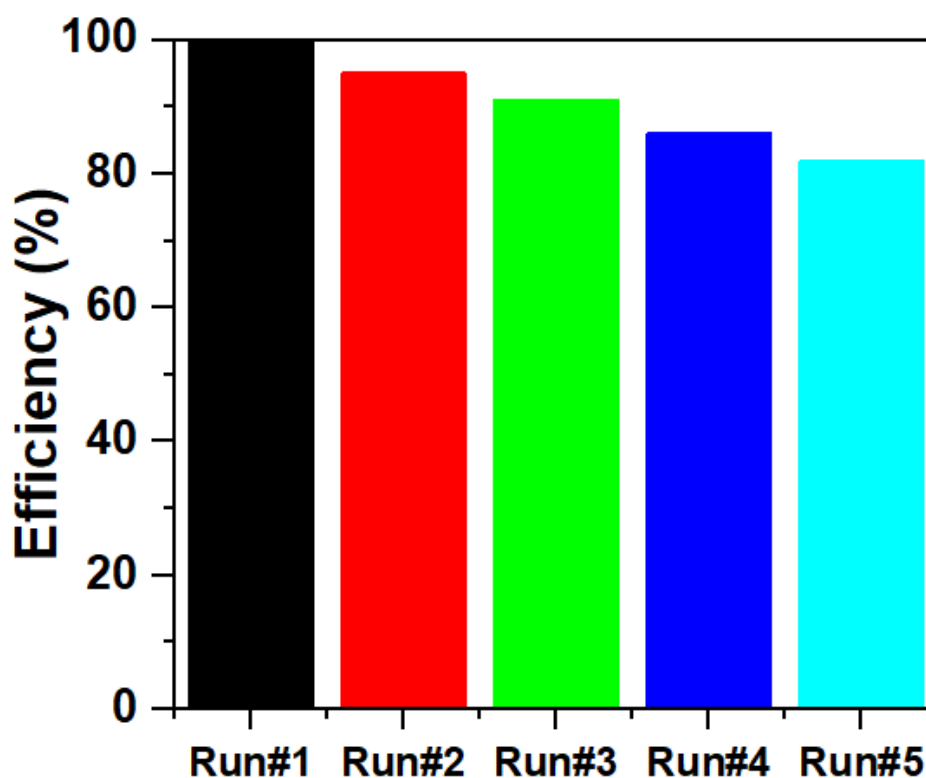
Fig. 12: The reusability test data for the $Cu_{1.7}Mo_{0.3}O_4$ catalyst after undergoing 5 reusability cycles.

Conclusions

This study focused on the processing and characterization of a highly effective copper molybdate catalyst for hydrogen evolution. Through the gelatin/sol-gel combustion method, $Cu_{1.7}Mo_{0.3}O_4$ and $Cu_{1.4}Mo_{0.6}O_4$ nanostructures were synthesized and investigated at two different concentrations. The structural, morphological, and optical properties of the nanocomposites were thoroughly examined using techniques such as X-ray diffraction and FTIR spectroscopy. The XRD data revealed the triclinic crystal structure system of

$Cu_{1.7}Mo_{0.3}O_4$ and orthorhombic $Cu_{1.4}Mo_{0.6}O_4$ system. The average crystalline size was obtained for $Cu_{1.7}Mo_{0.3}O_4$ to be 32.7 nm while 60.5 nm for $Cu_{1.4}Mo_{0.6}O_4$. The SEM images of $Cu_{1.7}Mo_{0.3}O_4$, and $Cu_{1.4}Mo_{0.6}O_4$ nanostructures have a plate-like morphology with a smooth surface. Nitrogen isotherm surface area analysis has shown that $Cu_{1.7}Mo_{0.3}O_4$, and $Cu_{1.4}Mo_{0.6}O_4$ have a high BET surface area, typically 53 and 502 m^2/g. The optical band gaps were determined to be 4.14 eV for $Cu_{1.7}Mo_{0.3}O_4$, while 3.91 eV for $Cu_{1.4}Mo_{0.6}O_4$. The $Cu_{1.7}Mo_{0.3}O_4$ sample demonstrated the highest level of activity in terms of hydrogen production from $NaBH_4$ methanolysis. The $Cu_{1.7}Mo_{0.3}O_4$ sample demonstrated the highest production rate of 23063 mL/g.min. The activation energies of $Cu_{1.7}Mo_{0.3}O_4$ and $Cu_{1.4}Mo_{0.6}O_4$ catalysts were calculated to be 12.42 and 22.64 kJ/mol. These findings will contribute to the development of effective catalysts for hydrogen evolution, opening new possibilities in renewable energy research.

Acknowledgement

Author Contributions

All the authors have equal contribution to the manuscript.

Ethics approval

Hereby, the corresponding author declares that the authors have thoroughly read the Journal Policy. Here, I declare that this contribution is original and has not been published anywhere. Also, I declare that this article doesn't contain any plagiarized materials.

Declaration of competing interest

The authors declare that they have no known competing financial interests or personal relationships that could have appeared to influence the work reported in this paper.

Availability of Data and Material

The data that support the findings of this study are available from the author upon reasonable request.

References

1. Zhu W, Zhang R, Qu F, Asiri AM, Sun X. Design and application of foams for electrocatalysis. ChemCatChem 2017;9:1721e43.
2. Li X, Zhang R, Luo Y, Liu Q, Lu S, Chen G, et al. A cobaltephosphorus nanoparticle decorated N-doped carbon nanosheet array for efficient and durable hydrogen evolution at alkaline pH. Sustain Energy Fuels 2020;4:3884e7.
3. Fakiolu E. A review of hydrogen storage systems based on boron and its compounds. Int J Hydrogen Energy 2004;29:1371e6.
4. Stern, Nicholas Herbert. The economics of climate change: the Stern review. cambridge University press, 2007.
5. Midilli, A., & Dincer, I. (2007). Key strategies of hydrogen energy systems for sustainability. International Journal of Hydrogen Energy, 32(5), 511-524.
6. Marrero-Alfonso, E. Y., Beaird, A. M., Davis, T. A., & Matthews, M. A. (2009). Hydrogen generation from chemical hydrides. Industrial & Engineering Chemistry Research, 48(8), 3703-3712.
7. Ogden, J. M., Kreutz, T. G., & Steinbugler, M. M. (2000). Fuels for fuel cell vehicles. Fuel Cells Bulletin, 3(16), 5-13.
8. Pehr, K. (1996). Aspects of safety and acceptance of LH2 tank systems in passenger cars. International Journal of Hydrogen Energy, 21(5), 387-395.
9. Ye, Y., Ahn, C. C., Witham, C., Fultz, B., Liu, J., Rinzler, A. G., ... & Smalley, R. E. (1999). Hydrogen adsorption and cohesive energy of single-walled carbon nanotubes. Applied physics letters, 74(16), 2307-2309.
10. Rangel, C. M., Fernandes, V. R., Slavkov, Y., & Bozukov, L. (2009). Novel hydrogen generator/storage based on metal hydrides. International journal of hydrogen energy, 34(10), 4587-4591.
11. Gross, K. J., Thomas, G. J., & Jensen, C. M. (2002). Catalyzed alanates for hydrogen storage. Journal of Alloys and Compounds, 330, 683-690.
12. Schlapbach, L., & Züttel, A. (2001). Hydrogen-storage materials for mobile applications. nature, 414(6861), 353-358.
13. Bakker, S. (2010). Hydrogen patent portfolios in the automotive industry–The search for promising storage methods. International Journal of Hydrogen Energy, 35(13), 6784-6793.
14. Diakov, V., Diwan, M., Shafirovich, E., & Varma, A. (2007). Mechanistic studies of combustion-stimulated hydrogen generation from sodium borohydride. Chemical engineering science, 62(18-20), 5586-5591.

15. Santos, D. M. F., & Sequeira, C. A. C. (2011). Sodium borohydride as a fuel for the future. Renewable and Sustainable Energy Reviews, 15(8), 3980-4001.
16. Strawser, D., Thangavelautham, J., & Dubowsky, S. (2014). A passive lithium hydride based hydrogen generator for low power fuel cells for long-duration sensor networks. international journal of hydrogen energy, 39(19), 10216-10229.
17. Liu, Y., Wang, X., Liu, H., Dong, Z., Cao, G., & Yan, M. (2014). Hydrogen generation from Mg–LiBH4 hydrolysis improved by AlCl3 addition. Energy, 68, 548-554.
18. Chinnappan, A., Kang, H. C., & Kim, H. (2011). Preparation of PVDF nanofiber composites for hydrogen generation from sodium borohydride. Energy, 36(2), 755-759.
19. Arthur, E. E., Li, F., Momade, F. W., & Kim, H. (2014). Catalytic hydrolysis of ammonia borane for hydrogen generation using cobalt nanocluster catalyst supported on polydopamine functionalized multiwalled carbon nanotube. Energy, 76, 822-829.
20. Chen Y, Shi Y, Liu X, Zhang Y. Preparation of polyvinylidene fluoride-nickel hollow fiber catalytic membranes for hydrogen generation from sodium borohydride. Fuel 2015;140:685e92.
21. Liu BH, Li ZP. A review: hydrogen generation from borohydride hydrolysis reaction. J Power Sources 2009;187:527e34.
22. Lu YC, Chen MS, Chen YW. Hydrogen generation by sodium borohydride hydrolysis on nanosized CoB catalysts supported on TiO2, Al2O3 and CeO2. Int J Hydrogen Energy 2012;37:4254e8.
23. Chinnappan, A., Appiah-Ntiamoah, R., Chung, W. J., & Kim, H. (2016). Ionic liquid functionalized graphene oxide decorated with copper oxide nanostructures towards H2 generation from sodium borohydride. International Journal of Hydrogen Energy, 41(33), 14491-14497.
24. Saka, C., Kaya, M., & Bekiroğullari, M. (2020). Chlorella vulgaris microalgae strain modified with zinc chloride as a new support material for hydrogen production from NaBH4 methanolysis using CuB, NiB, and FeB metal catalysts. International journal of hydrogen energy, 45(3), 1959-1968.
25. Dönmez, F., & Ayas, N. (2021). Synthesis of Ni/TiO2 catalyst by sol-gel method for hydrogen production from sodium borohydride. International Journal of Hydrogen Energy, 46(57), 29314-29322.
26. Ma, J., Wei, H., Liu, Y., Ren, X., Li, Y., Wang, F., ... & Wei, S. (2020). Application of Co3O4-based materials in electrocatalytic hydrogen evolution reaction: a review. International Journal of Hydrogen Energy, 45(41), 21205-21220.
27. Ji, J., Deng, K., Li, J., Zhang, Z., Duan, X., & Huang, H. (2021). In situ transformation of 3D Co3O4 nanoparticles to 2D nanosheets with rich surface oxygen vacancies to boost hydrogen generation from NaBH4. Chemical Engineering Journal, 424, 130350.
28. Wei, L., Cao, X., Ma, M., Lu, Y., Wang, D., Zhang, S., & Wang, Q. (2018). Co3O4 nanowires as efficient catalyst precursor for hydrogen generation from sodium borohydride hydrolysis. Functional Materials Letters, 11(01), 1850018.
29. Patil, K. N., Prasad, D., Manoorkar, V. K., Nabgan, W., Nagaraja, B. M., & Jadhav, A. H. (2021). Engineered nano-foam of tri-metallic (FeCuCo) oxide catalyst for enhanced hydrogen generation via NaBH4 hydrolysis. Chemosphere, 281, 130988.
30. Tan, W., & Luan, J. (2020). Investigation into the synthesis conditions of CuMoO 4 by an in situ method and its photocatalytic properties under visible light irradiation. RSC advances, 10(16), 9745-9759.

31. Hassani, H. O., Akouibaa, M., Rakass, S., Abboudi, M., El Bali, B., Lachkar, M., & Al Wadaani, F. (2021). A simple and cost-effective new synthesis method of copper molybdate CuMoO4 nanoparticles and their catalytic performance. Journal of Science: Advanced Materials and Devices, 6(3), 501-507.

32. Taha, T. A., Saad, R., Zayed, M., Shaban, M., & Ahmed, A. M. (2023). Tuning the surface morphologies of ZnO nanofilms for enhanced sensitivity and selectivity of CO2 gas sensor. Applied Physics A, 129(2), 115.

33. Manzoor, S., Abid, A. G., Aman, S., Abdullah, M., Rashid, A. R., Ali, H. M., ... & Taha, T. A. (2022). Facile synthesis of CoFePO4 on eggshell membrane for oxygen evolution reaction and supercapacitor applications. Ceramics International, 48(24), 36975-36982.

34. Seevakan, K., Manikandan, A., Devendran, P., Slimani, Y., Baykal, A., & Alagesan, T. (2018). Structural, morphological and magneto-optical properties of CuMoO4 electrochemical nanocatalyst as supercapacitor electrode. Ceramics International, 44(16), 20075-20083.

35. Tan, W., & Luan, J. (2020). Investigation into the synthesis conditions of CuMoO 4 by an in situ method and its photocatalytic properties under visible light irradiation. RSC advances, 10(16), 9745-9759.

36. Rani, B. J., Swathi, S., Yuvakkumar, R., Ravi, G., Kumar, P., Babu, E. S., ... & Velauthapillai, D. (2021). Solvothermal synthesis of CoMoO 4 nanostructures for electrochemical applications. Journal of Materials Science: Materials in Electronics, 32, 5989-6000.

37. Zhenyang, Wang., Jianliang, Zhang., Jianliang, Zhang., Baojun, Zhao., Hongyuan, Fu., Jing, Pang. (2021). Effect of pore characteristics on hydrogen reduction kinetics based on a novel analysis approach combined model-fitting and iso-conversion. International Journal of Hydrogen Energy, 46(45):23164-23173.

38. Xie, T., Wang, J., Ding, F., Zhang, A., Li, W., Guo, X., & Song, C. (2017). CO2 hydrogenation to hydrocarbons over alumina-supported iron catalyst: Effect of support pore size. Journal of CO2 Utilization, 19, 202-208.

39. Shimizu, T., Ota, M., Sato, Y., & Inomata, H. (2015). Effect of pore structure on catalytic properties of mesoporous silica supported rhodium catalysts for the hydrogenation of cinnamaldehyde. Chemical Engineering Research and Design, 104, 174-179.

40. Maeda, K., Teramura, K., Lu, D., Takata, T., Saito, N., Inoue, Y., & Domen, K. (2006). Photocatalyst releasing hydrogen from water. Nature, 440(7082), 295-295.

41. Brugger, P. A., Cuendet, P., & Graetzel, M. (1981). Ultrafine and specific catalysts affording efficient hydrogen evolution from water under visible light illumination. Journal of the American Chemical Society, 103(11), 2923-2927.

42. Aleksandrov, H. A., Kozlov, S. M., Schauermann, S., Vayssilov, G. N., & Neyman, K. M. (2014). How absorbed hydrogen affects the catalytic activity of transition metals. Angewandte Chemie, 126(49), 13589-13593.

43. Borgschulte, A., Westerwaal, R. J., Rector, J. H., Schreuders, H., Dam, B., & Griessen, R. (2006). Catalytic activity of noble metals promoting hydrogen uptake. Journal of Catalysis, 239(2), 263-271.

44. Borgschulte, A., Lohstroh, W., Westerwaal, R. J., Schreuders, H., Rector, J. H., Dam, B., & Griessen, R. (2005). Combinatorial method for the development of a catalyst promoting hydrogen uptake. Journal of alloys and compounds, 404, 699-705.

45. Keerthana, S. P., Rani, B. J., Yuvakkumar, R., Ravi, G., Shivatharsiny, Y., Babu, E. S., ... & Velauthapillai, D. (2021). Copper molybdate nanoparticles for electrochemical water splitting application. International Journal of Hydrogen Energy, 46(11), 7701-7711.

46. Alshammari, A. H., Alshammari, K., Alhassan, S., Alshammari, M., Alotaibi, T., Alanzy, A. O., & Taha, T. A. M. (2023). Low temperature sol-gel synthesis of copper zinc ferrite for hydrogen catalytic hydrolysis of sodium borohydride. Materials Chemistry and Physics, 308, 128287.

47. Alshammari, M., Alhassan, S., Alshammari, K., Alotaibi, T., Alshammari, A. H., Alotibi, S., ... & Ismael, A. (2023). Hydrogen catalytic performance of hybrid Fe3O4/FeS2/g-C3N4 nanocomposite structures. Diamond and Related Materials, 138, 110214.

48. Ijeh, R. O., Nwanya, A. C., Nkele, A. C., Madiba, I. G., Bashir, A. K. H., Ekwealor, A. B. C., ... & Ezema, F. (2020). Optical, electrical and magnetic properties of copper doped electrodeposited MoO3 thin films. Ceramics International, 46(8), 10820-10828.

49. San Martín, S., Rivero, M. J., & Ortiz, I. (2020). Unravelling the mechanisms that drive the performance of photocatalytic hydrogen production. Catalysts, 10(8), 901.

50. Waterhouse, G. I. N., Wahab, A. K., Al-Oufi, M., Jovic, V., Anjum, D. H., Sun-Waterhouse, D., ... & Idriss, H. (2013). Hydrogen production by tuning the photonic band gap with the electronic band gap of TiO2. Scientific Reports, 3(1), 2849.

51. Saka, C., & Balbay, A. (2019). Influence of process parameters on enhanced hydrogen generation via semi-methanolysis and semi-ethanolysis reactions of sodium borohydride using phosphoric acid. International Journal of Hydrogen Energy, 44(57), 30119-30126.

52. C. Saka, Efficient and durable H2 production from NaBH4 methanolysis using N doped hybrid g-C3N4-SiO2 composites with ammonia as a nitrogen source, Fuel 324 (2022), 124594.

53. Yang, C. C., Chen, M. S., & Chen, Y. W. (2011). Hydrogen generation by hydrolysis of sodium borohydride on CoB/SiO2 catalyst. International Journal of Hydrogen Energy, 36(2), 1418-1423.

54. Andrieux, J., Demirci, U. B., & Miele, P. (2011). Langmuir–Hinshelwood kinetic model to capture the cobalt nanoparticles-catalyzed hydrolysis of sodium borohydride over a wide temperature range. Catalysis today, 170(1), 13-19.

55. Alshammari, K., Alotaibi, T., Alshammari, M., Alhassan, S., Alshammari, A. H., & Taha, T. A. M. (2023). Synthesis of Sulfur@ g-C3N4 and CuS@ g-C3N4 Catalysts for Hydrogen Production from Sodium Borohydride. Materials, 16(12), 4218.

56. Alshammari, Majed, Sultan Alhassan, Khulaif Alshammari, Turki Alotaibi, Taha Abdel Mohaymen Taha, Alhulw H. Alshammari, and Ali Ismael. "Synthesis of CaCO3/Cu2O/GO Nanocomposite Catalysts for Hydrogen Production from NaBH4 Methanolysis." Catalysts 13, no. 6 (2023): 1010.

57. Shen, X., Wang, Q., Wu, Q., Guo, S., Zhang, Z., Sun, Z., ... & Ding, W. (2015). CoB supported on Ag-activated TiO2 as a highly active catalyst for hydrolysis of alkaline NaBH4 solution. Energy, 90, 464-474.

58. Wei, Y., Wang, R., Meng, L., Wang, Y., Li, G., Xin, S., ... & Zhang, K. (2017). Hydrogen generation from alkaline NaBH4 solution using a dandelion-like Co–Mo–B catalyst supported on carbon cloth. international journal of hydrogen energy, 42(15), 9945-9951.

59. Patil, K.N.; Prasad, D.; Bhanushali, J.T.; Kim, H.; Atar, A.B.; Nagaraja, B.M.; Jadhav, A.H. Sustainable Hydrogen Generation by Catalytic Hydrolysis of NaBH4 Using Tailored Nanostructured Urchin-like CuCo2O4 Spinel Catalyst. Catal. Lett. 2019, 150, 586–604.

60. Lai, J. L., Luo, W. J., Kuan, Y. D., & Zhang, P. J. (2021). The effect of hydrogen production rate of the via different preparation of Co-based catalyst with sodium borohydride. Catalysts, 11(5), 528.

61. Kılınç, D., & Şahin, Ö. (2019). Effective TiO2 supported Cu-Complex catalyst in NaBH4 hydrolysis reaction to hydrogen generation. International Journal of Hydrogen Energy, 44(34), 18858-18865.

62. Şahin, Ö., Karakaş, D. E., Kaya, M., & Saka, C. (2017). The effects of plasma treatment on electrochemical activity of Co–B–P catalyst for hydrogen production by hydrolysis of NaBH4. Journal of the Energy Institute, 90(3), 466-475.

63. Avci Hansu, T., Sahin, O., Caglar, A., & Kivrak, H. (2020). A remarkable Mo doped Ru catalyst for hydrogen generation from sodium borohydride: the effect of Mo addition and estimation of kinetic parameters. Reaction Kinetics, Mechanisms and Catalysis, 131, 661-676.

64. Abdulaziz, Fahad, Salman Latif, and Taha Abdel Mohaymen Taha. "Preparation of Co–CaCO3 catalysts for improved hydrogen production from sodium borohydride." International Journal of Hydrogen Energy 56 (2024): 271-279.

65. Scott Fogler, H. " Elements of Chemical Reaction Engineering (5th ed.)." Prentice Hall (2015).

66. Davis, M. E., & Davis, R. J. (Eds.). "Fundamentals of Chemical Reaction Engineering." McGraw-Hill Education (2013).